Dalton Transactions

ROYAL SOCIETY OF CHEMISTRY

COMMUNICATION

View Article Online
View Journal | View Issue





Cite this: *Dalton Trans.*, 2025, **54**, 8405

Received 4th April 2025,
Accepted 26th April 2025

DOI: 10.1039/d5dt00817d

rsc.li/dalton

# Structure and ion conducting properties of mixed-alkali $Na_{3-x}Li_xInCl_6$ solid electrolytes†

Dat Le Thanh, [a,b,c] Long Hoang Bao Nguyen, [b,d] Emmanuelle Suard [a] and Romain Berthelot *[b,d]

**Li substitution and its impact on the structures and ion transport of $Na_{3-x}Li_xInCl_6$ polymorphs, synthesized *via* ball-milling and further annealing, were investigated. Despite a solubility limit of $x$ = 0.6, Li incorporation seems to form a connected $Li^+$ network to enhance the ionic conductivity of the resulting materials.**

All-solid-state batteries (ASSBs) have attracted considerable interest in recent years thanks to their enhanced energy density, improved safety, and extended lifetime. The development of ASSBs has stimulated the discovery of new inorganic materials possessing high ionic conductivity, even at ambient temperature.[1] Depending on the nature of the anion, inorganic solid-state electrolytes (SSEs) are usually classified into oxides, sulphides, or halides, with the latter being well recognized thanks to their high oxidation stability and excellent mechanical flexibility required for material processing and cell assembly.[2–4] The development of halide SSEs has advanced rapidly since the pioneering work of Asano *et al.*, reporting $Li_3YCl_6$ and $Li_3YBr_6$ that possess room-temperature $Li^+$ conductivities of up to 0.5 and 1.7 mS $cm^{-1}$, respectively.[5] Since then, different families of halide-based $Li^+$ SSEs have been thoroughly investigated, including aliovalent substitution solid solutions, such as $Li_{3-x}In_{1-x}Zr_xCl_6$, which exhibits a high ionic conductivity of up to 1.25 mS $cm^{-1}$ for $x$ = 0.4.[6]

Besides halide-based $Li^+$ SSEs, the number of studies on $Na^+$ counterparts has surged in the last few years. The most commonly investigated halide-based $Na^+$ SSEs are $Na_3MX_6$ where M = Sc, Y, In, and Sm–Lu and X = Cl, Br, or I; nonetheless, most of them exhibit relatively low ionic conductivity at ambient temperature.[7–10] Different strategies, including compositional and structural modifications, have been carried out to improve their conducting properties. One of the most widely adopted approaches is aliovalent substitution at the transition metal site, which can enhance $Na^+$ conductivity by about three or four orders of magnitude compared with undoped compositions. For instance, $Na_2ZrCl_6$ exhibits an $Na^+$ conductivity of $6.9 \times 10^{-5}$ mS $cm^{-1}$, compared to $6.6 \times 10^{-2}$ and $3.5 \times 10^{-2}$ mS $cm^{-1}$ of $Na_{2.25}Zr_{0.75}Y_{0.25}Cl_6$ and $Na_{2.4}Zr_{0.6}Er_{0.4}Cl_6$, respectively.[11–13] The other strategy involves anionic mixing to modify bond strength between the alkali and halogen atoms, thereby facilitating ion conduction.[14,15] This approach was reported for halide-based $Na^+$ SSEs, including $Na_3GdBr_xI_{6-x}$ [16] and $Na_3InCl_{6-x}Br_x$,[10] though little improvement in the ionic conductivity was observed.

The structures of halide-based $Li^+/Na^+$ SSEs, $A_xMX_n$, have several similarities. Indeed, they can be described as a close packed lattice of $X^-$ anions, while the cations, $Li^+/Na^+$ and $M^{n+}$, occupy the available interstitial sites. Both hexagonal and cubic close packed anion lattices have been observed; nonetheless, subtle structural distortions can occur depending on the amount of alkali vacancies and the charge and ionic radii of alkali, metal, and halide ions, leading to a structural diversity of the resulting compound. The difference in the energy of hexagonal and cubic lattices is subtle and thermal treatment can lead to a structural conversion between the two forms. It was suggested that cubic packing offers more favorable interstitial connectivity and diffusion pathways than hexagonal packing, potentially resulting in higher ionic conductivity.[17] Alkali vacancies and aliovalent and isovalent substitution on the metal/anion site are the three degrees of freedom that are commonly used to monitor the structure and ionic conductivity of halide-based $Li^+/Na^+$ SSEs. Isovalent substitution on the alkali site also represents a degree of freedom that can directly affect the structure and conduction properties but is rarely reported in the literature.

In the present work, the impact of isovalent alkali substitution on the structure and ion transport properties of halide-

[a]*Institut Laue-Langevin (ILL), 38042 Grenoble, France*
[b]*ICGM, Univ. Montpellier, CNRS, ENSCM, 34095 Montpellier, France. E-mail: romain.berthelot@umontpellier.fr*
[c]*Alistore-European Research Institute, CNRS FR 3104, 80039 Amiens, France*
[d]*Réseau sur le Stockage électrochimique de l'énergie (RS2E), CNRS, 80039 Amiens, France*

†Electronic supplementary information (ESI) available: Experimental details, powder X-ray and neutron diffraction patterns, and electrochemical impedance spectra. See DOI: https://doi.org/10.1039/d5dt00817d

based SSEs will be investigated using $Na_{3-x}Li_xInCl_6$. The parental compound $Li_3InCl_6$ adopts a trigonal structure with a hexagonal packing lattice of $Cl^-$ while $Li^+$ and $In^{3+}$ occupy octahedral sites.[6,18] On the other hand, $Na_3InCl_6$ can adopt either the same trigonal structure or a monoclinic one, which is a distorted cubic packing lattice of $Cl^-$ with part of the $Na^+$ occupying the prismatic site.[10,19] The existence of two different polymorphs for $Na_3InCl_6$ allows an insightful study on the solubility limit and impacts of $Li^+$ substitution in each structure. Several $Na_{3-x}Li_xInCl_6$ compounds with different Li contents are synthesized using mechanochemistry, which might favor the formation of metastable phases, followed by a subsequent thermal treatment to obtain thermodynamically stable products. A combination of powder X-ray diffraction (PXRD), neutron diffraction (ND), and electrochemical impedance spectroscopy (EIS) is employed to investigate the solubility limit, structural modifications and conduction properties of the resulting compounds.

A series of $Na_{3-x}Li_xInCl_6$ ($0 \le x \le 1.5$) compositions was prepared using mechanochemistry. Up to $x = 0.6$, the PXRD patterns of the as-obtained samples can be indexed using the monoclinic structure ($P2_1/n$ space group), in which the $Cl^-$ lattice forms a distorted cubic close packing structure while $In^{3+}$ occupies octahedral sites; $Na^+$ and $Li^+$ are distributed over octahedral and prismatic sites (Fig. 1a and c). The $Na/LiCl_6$ trigonal prisms and octahedra are inter-connected *via* corner- and edge-sharing linkages, creating a tri-dimensional diffusion pathway for alkali ions. The cell parameters obtained from Rietveld refinement (Fig. 2a and c) show that the variation in lattice parameters upon $Li^+$ substitution is subtle; nonetheless, a linear contraction of the unit cell is observed up to $x = 0.6$, suggesting a lithium incorporation process. From $x = 0.9$ up to $x = 1.5$, Bragg peaks of the desired phase become progressively broader and less intense (Fig. S2†), indicating a decrease in crystallinity. Furthermore, new peaks corresponding to impurities are observed, suggesting that a solid solution might not have been formed in this compositional range.

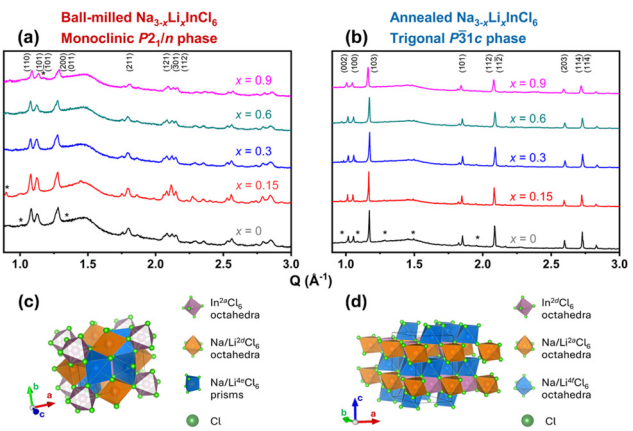


**Fig. 1** PXRD patterns and crystal structures of the $Na_{3-x}Li_xInCl_6$ ($0 \le x \le 0.9$) series synthesized by mechanochemistry (a and c) followed by annealing at 200 °C (b and d). The low-intensity peaks, marked with * in one representative pattern, may indicate the presence of impurities, although they cannot be attributed to any specific compound.

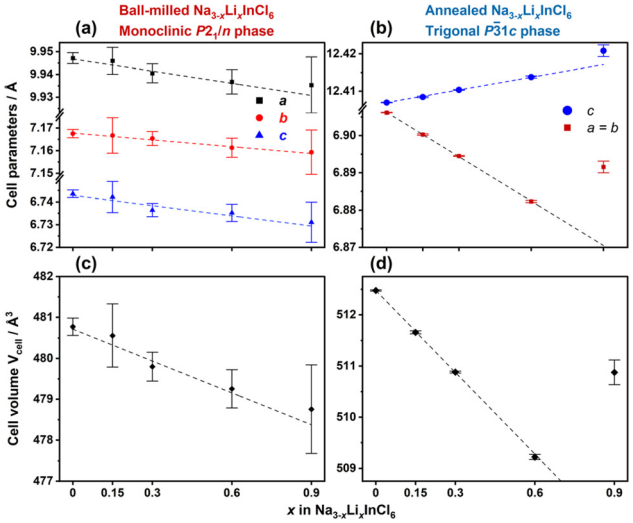


**Fig. 2** Evolution of cell parameters and cell volume for the $Na_{3-x}Li_xInCl_6$ ($0 \le x \le 0.9$) series determined by Rietveld refinement of the PXRD patterns. Samples were synthesized by ball-milling (a and c) followed by thermal treatment at 200 °C (b and d).

As thermal treatment can induce a significant impact on the structures and transport properties of mechanochemically prepared chloride SSEs,[10,19] an annealing process at 200 °C under vacuum was carried out on the as-obtained ball-milled $Na_{3-x}Li_xInCl_6$ samples ($0 \le x \le 1.5$). The PXRD patterns of the annealed samples show an evident phase transformation with an enhanced crystallinity (Fig. 1b). Most diffraction peaks can be indexed using the trigonal polymorph ($P\bar{3}1c$ space group) of $Na_3InCl_6$. This observation agrees with previous studies, showing that monoclinic $Na_3InCl_6$ would convert to a trigonal polymorph upon thermal treatment.[10,19] Unlike the monoclinic $P2_1/n$ space group, all metal sites in the trigonal $P\bar{3}1c$ phase group are octahedrally coordinated by chloride ions. The structure consists of two distinct alternating layers stacked along the *c*-axis: one contains only edge-sharing $Na/Li^{4f}Cl_6$ octahedra and the other contains $Na/Li^{2a}Cl_6$ and $In^{2d}Cl_6$ octahedra alternately linked by edge-sharing to form honeycomb layers (Fig. 1d). The $Na/LiCl_6$ octahedra between the two layers are connected *via* corner-sharing, creating here also a tri-dimensional diffusion pathway for alkali ions.

Rietveld refinements of PXRD data from thermally treated $Na_{3-x}Li_xInCl_6$ compositions show an expansion along the *c*-axis and a contraction in the (*ab*) plane upon $Li^+$ substitution. A linear evolution in the cell parameters consistent with Vegard's law is observed only until the composition $x = 0.6$. In this low $Li^+$ incorporation range, the mixed-alkali $Na_{3-x}Li_xInCl_6$ is thermodynamically stable as no impurity phase emerges upon heating. These results indicate the formation of solid solutions up to 20% ($x = 0.6$) in both monoclinic and trigonal $Na_{3-x}Li_xInCl_6$ polymorphs, despite the difference in the ionic radius of $Li^+$ and $Na^+$ (0.76 *vs.* 1.02 Å).[20]

In order to understand the impact of $Li^+$ substitution on the structure and ion conducting properties, insightful information on $Li^+$ and $Na^+$ site occupation is essential. The high crystallinity of trigonal $Na_{3-x}Li_xInCl_6$ compositions enables the use of the diffraction technique for Na/Li distribution analysis. Since $^7Li$ possesses a negative coherent scattering length, in contrast to the positive values for Na, Cl, and In,[21] ND is suitable for probing the Li position and investigating site preference for both alkali ions between two crystallographic sites (2*a* and 4*f*). An indirect approach, including ND pattern simulations for different scenarios of alkali ion distribution and comparison with experimental patterns, is used. Simulated patterns for $Na_{3-x}Li_xInCl_6$ ($x$ = 0.15, 0.3, and 0.6) are generated according to three scenarios: (1) all lithium at the 2*a* site, (2) all lithium at the 4*f* site, and (3) lithium evenly distributed between both sites.

For each composition, most diffraction peaks overlap significantly (Fig. S5†), except in the low-Q region where the (002) and (100) reflections exhibit notable intensity differences (Fig. 3). These differences become more pronounced as the $Li^+$ content increases. Comparison with the experimental ND data indicates that the extreme case, where $Li^+$ occupies only one site exclusively, can qualitatively be ruled out (Fig. 3 and S5†). Due to significant peak overlap in the simulated patterns and weak intensities in the region of interest, refining exact site occupation factors was challenging. However, the indirect simulation comparison approach was sufficiently reliable to suggest that both alkali ions likely occupy both sites, though their proportions remain undetermined.

The occupation of $Li^+$ in both 2*a* and 4*f* sites may help explain the limited solubility of $Li^+$ in an $Na_3InCl_6$ trigonal structure. At a low degree of substitution ($x \leq 0.6$), the replacement of $Na^+$ by $Li^+$ would lead to a contraction of cell parameters; however, the interstitial site would be big enough to accommodate both $Na^+$ and $Li^+$. For more Li-rich compositions, the contraction of the cell parameters and the size of the interstitial sites would be so great that $Na^+$ could not be fit in the structure.

To further understand the dual-site occupation of $Li^+$ and its effect on the conduction properties within the solid solution $Na_{3-x}Li_xInCl_6$ ($x \leq 0.6$), EIS was used. As electronic conductivity is considerably lower than ionic conductivity (Fig. S7, Tables S7 and S8†), only ionic contributions are considered in impedance analysis. The impedance spectra of all the samples show a suppressed semicircle, corresponding to the ionic conduction, followed by the capacitive blocking behavior of the stainless-steel electrodes (Fig. 4a, b and S6†). In this case, bulk and grain boundary contributions to the impedance cannot be deconvoluted; therefore, the values of reported conductivities herein represent the total ionic conductivities (Table S7†). All ball-milled and annealed phases at each composition exhibit Arrhenius behavior from 30 °C to 70 °C, though a deviation is observed at 80 °C. The ionic conductivity values of both $Na_3InCl_6$ polymorphs at 30 °C are of the same order of magnitude as those reported in other studies, both around $1.4 \times 10^{-5}$ mS $cm^{-1}$, indicating that $Na_3InCl_6$ is an ionic insulator. Upon $Li^+$ substitution, the ionic conductivity gradually increases. For instance, a 10% $Li^+$ substitution ($x$ = 0.3) results in small improvements, with ionic conductivities of $8.6 \times 10^{-5}$ and $4.9 \times 10^{-5}$ mS $cm^{-1}$ at 30 °C for the monoclinic and trigonal phases, respectively. At $Na^+$-rich compositions ($x \leq 0.3$), the

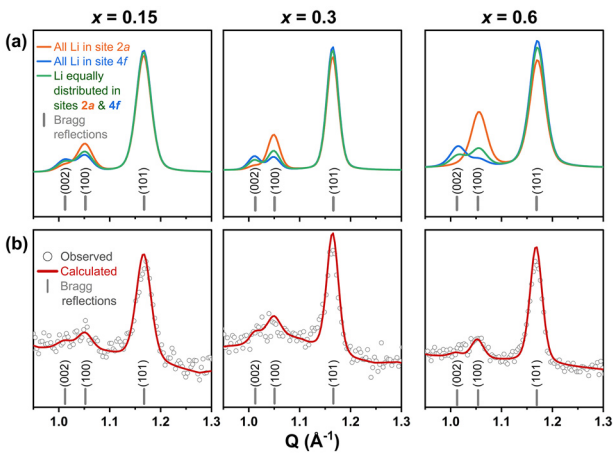


**Fig. 3** Simulated (a) and experimental (b) ND patterns for the three compositions of $Na_{3-x}In_xCl_6$ in the low-*Q* region. For each composition, three simulated ND patterns correspond to different lithium distributions between the 2*a* and 4*f* sites.

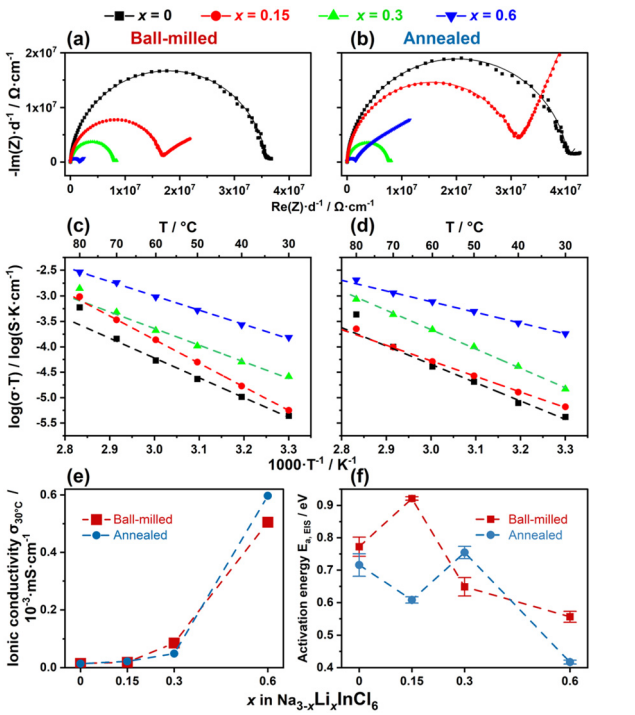


**Fig. 4** Representative Nyquist plots at 50 °C (a and b) and Arrhenius plots from the temperature-dependent impedance (c and d), corresponding to the ball-milled and annealed samples in the $Na_{3-x}Li_xInCl_6$ series. Comparison of ionic conductivities at 30 °C (e) and activation energies for ionic conduction (f) of these samples.

ionic conductivities of both polymorphs are of similar magnitude across the whole temperature range (30–80 °C), indicating that the packing sequence of $Cl^-$ has little impact on the ionic conductivity (Fig. 4c and d).

Remarkably, higher lithium substitution of 20% ($x$ = 0.6) leads to a conductivity enhancement by one order of magnitude, reaching $5.1 \times 10^{-4}$ and $6.0 \times 10^{-4}$ mS cm$^{-1}$ at 30 °C for the monoclinic and trigonal phases, respectively. This significant gain in ionic conductivity could be contributed by the enhanced motion of both $Na^+$ and $Li^+$ ions; nonetheless, the contribution from $Li^+$ is expected to be more significant than that from $Na^+$. As illustrated in Fig. 4e, the ionic conductivity of $Na_{3-x}Li_xInCl_6$ ($x \leq 0.6$) does not increase linearly with the amount of $Li^+$ present in the structure, but its evolution follows an exponential trend. This behaviour suggests that $Na^+$ in $Na_{3-x}Li_xInCl_6$ participates negligibly in ion conduction, but the ionic conductivity predominantly arises from $Li^+$ motion. At a low substitution amount, each $Li^+$ site is surrounded by $In^{3+}$ or $Na^+$, and thus little improvement in the ionic conductivity is observed. As the substitution degree increases, due to the occupation of $Li^+$ at both sites, $Li^+$ might form a 3D network, creating a diffusion pathway for $Li^+$ and leading to a significant conductivity enhancement. Additionally, both phases of $Na_{2.4}Li_{0.6}InCl_6$ possess the lowest activation energy, indicating that this composition might contain sufficient $Li^+$ to create a connected $Li^+$ network to facilitate $Li^+$ diffusion. The ionic conductivity of the annealed sample is slightly higher than the one obtained from ball-milling, implying that the hexagonal packing of $Cl^-$ might facilitate the diffusion in this case. This is an interesting example showing that $Na^+$ in these mixed-alkali compositions would be immobile, but $Li^+$ would be mobile if the threshold amount of $Li^+$ was reached. Li/Na mixed compositions are also observed in some layered oxides,[22] and the resulting compounds can be used as electrode materials for Li- or Na-ion batteries. The flexibility in the structural properties of $A_3InCl_6$ and layered oxides could be due to the similar stacking sequence of the $InCl_6/MO_6$ structural units, and the size of the interstitial sites can vary to accommodate the guest ions.

## Conclusions

Several mixed-alkali solid solutions of $Na_{3-x}Li_xInCl_6$ were prepared *via* ball-milling and subsequent annealing, showing a phase transition from monoclinic to trigonal upon annealing. Lattice parameters evolve linearly up to a $Li^+$ solubility limit at $x$ = 0.6, beyond which interstitial contraction and ion size mismatch hinder further incorporation. ND revealed that the newly introduced lithium occupies both alkali sites. EIS analysis shows an exponential increase of ionic conductivity with higher $Li^+$ content, suggesting that the smaller lithium ions become progressively more connected and mobile, thus dominating the transport behaviour. These findings demonstrate the potential of alkali substitution to tailor the structure and ionic transport properties of halide-based solid-state electrolytes.

## Data availability

The data supporting this article have been included as part of the ESI.†

## Conflicts of interest

There are no conflicts to declare.

## Acknowledgements

As a part of the DESTINY PhD program, this publication acknowledges funding from the European Union's Horizon2020 Research and Innovation Program under the Marie Skłodowska-Curie Actions COFUND (Grant Agreement #945357). The authors acknowledge MSPD staff at ALBA synchrotron for help and data collection on the 2023097745 proposal beamtime.

## References

1 T. Famprikis, P. Canepa, J. A. Dawson, M. S. Islam and C. Masquelier, *Nat. Mater.*, 2019, **18**, 1278–1291.
2 H. Kwak, S. Wang, J. Park, Y. Liu, K. T. Kim, Y. Choi, Y. Mo and Y. S. Jung, *ACS Energy Lett.*, 2022, **7**, 1776–1805.
3 L. Huang, L. Zhang, J. Bi, T. Liu, Y. Zhang, C. Liu, J. Cui, Y. Su, B. Wu and F. Wu, *Energy Mater. Adv.*, 2024, **5**, 0092.
4 X. Nie, J. Hu and C. Li, *Interdiscip. Mater.*, 2023, **2**, 365–389.
5 T. Asano, A. Sakai, S. Ouchi, M. Sakaida, A. Miyazaki and S. Hasegawa, *Adv. Mater.*, 2018, **30**, 1803075.
6 B. Helm, R. Schlem, B. Wankmiller, A. Banik, A. Gautam, J. Ruhl, C. Li, M. R. Hansen and W. G. Zeier, *Chem. Mater.*, 2021, **33**, 4773–4782.
7 G. Meyer, S. Peter Ax, T. Schleid and M. Irmler, *Z. Anorg. Allg. Chem.*, 1987, **554**, 25–33.
8 M. S. Wickleder and G. Meyer, *Z. Anorg. Allg. Chem.*, 1995, **621**, 457–463.
9 A. Bohnsack and G. Meyer, *Z. Anorg. Allg. Chem.*, 1996, **622**, 173–178.
10 T. Zhao, M. A. Kraft and W. G. Zeier, *Inorg. Chem.*, 2023, **62**, 11737–11745.
11 H. Kwak, J. Lyoo, J. Park, Y. Han, R. Asakura, A. Remhof, C. Battaglia, H. Kim, S.-T. Hong and Y. S. Jung, *Energy Storage Mater.*, 2021, **37**, 47–54.
12 E. A. Wu, S. Banerjee, H. Tang, P. M. Richardson, J.-M. Doux, J. Qi, Z. Zhu, A. Grenier, Y. Li, E. Zhao, G. Deysher, E. Sebti, H. Nguyen, R. Stephens, G. Verbist, K. W. Chapman, R. J. Clément, A. Banerjee, Y. S. Meng and S. P. Ong, *Nat. Commun.*, 2021, **12**, 1256.
13 R. Schlem, A. Banik, M. Eckardt, M. Zobel and W. G. Zeier, *ACS Appl. Energy Mater.*, 2020, **3**, 10164–10173.
14 P. Till, M. T. Agne, M. A. Kraft, M. Courty, T. Famprikis, M. Ghidiu, T. Krauskopf, C. Masquelier and W. G. Zeier, *Chem. Mater.*, 2022, **34**, 2410–2421.

 

15 X. Zhang, K. C. Phuah and S. Adams, *Chem. Mater.*, 2021, **33**, 9184–9193.
16 A. Bohnsack and G. Meyer, *Z. Anorg. Allg. Chem.*, 1997, **623**, 837–843.
17 X. Li, J. T. Kim, J. Luo, C. Zhao, Y. Xu, T. Mei, R. Li, J. Liang and X. Sun, *Nat. Commun.*, 2024, **15**, 53.
18 X. Li, J. Liang, J. Luo, M. Norouzi Banis, C. Wang, W. Li, S. Deng, C. Yu, F. Zhao, Y. Hu, T.-K. Sham, L. Zhang, S. Zhao, S. Lu, H. Huang, R. Li, K. R. Adair and X. Sun, *Energy Environ. Sci.*, 2019, **12**, 2665–2671.
19 T. Zhao, A. N. Sobolev, R. Schlem, B. Helm, M. A. Kraft and W. G. Zeier, *ACS Appl. Energy Mater.*, 2023, **6**, 4334–4341.
20 R. D. Shannon, *Acta Crystallogr., Sect. A*, 1976, **32**, 751–767.
21 *Neutron data booklet*, ed. A. J. Dianoux and Institut Laue-Langevin, Old City, Philadelphia, PA, 2nd edn, 2003.
22 C. Vallée, M. Saubanère, P. Sanz-Camacho, Y. Biecher, B. Fraisse, E. Suard, G. Rousse, D. Carlier and R. Berthelot, *Inorg. Chem.*, 2019, **58**, 11546–11552.